HETEROEPITAXY OF PEROVSKITE FERROELECTRICS ON SILICON - A PATH TO SILICON-INTEGRATED FERROELECTRICS

CONF-960813--3

R.A. McKee, F.J. Walker, and M.F. Chisholm
Oak Ridge National Laboratory, Oak Ridge, TN 37831-0618

Abstract

We have studied the thin-film heteroepitaxy between simple perovskite oxides and silicon as it is accomplished with molecular beam epitaxy growth techniques. Interface chemistry and electrostatics play critical roles in determining whether a commensurate interface develops. Submonolayer silicides are the required precursors for the transition to commensurate epitaxial oxide structures in these systems. We illustrate this approach with $BaTiO_3$; high crystalline perfection is achieved and resistivities as high as 10^{13} ohm-cm can be developed for $BaTiO_3$ MOS capacitors on (001) silicon. The epitaxy is (100)$BaTiO_3$// (001)Si with [001]$BaTiO_3$ aligned in plane with the polar axis along the [110] of silicon. This epitaxy is dominated by a strong propensity for barium to order along the [110] of silicon during the submonolayer silicide formation. This commensurate heteroepitaxial growth leads to a truly monolithic crystal and attendant properties.

Introduction

A monolithic integration of semiconductor and perovskite oxide materials is a challenging scientific problem with technological implications that hinge on whether a true synergism of the dissimilar materials properties is realized. For example, with ferroelectric members of the perovskites like $BaTiO_3$, the electric polarization of the crystal is the means by which the coupling between the semiconductor and the ionic oxide occurs. Ferroelectric polarization in the oxide sets up charge compensation in the semiconductor and drives the coupling, or synergism, of the dissimilar materials. A commensurate interface ties up dangling bonds at the semiconductor truncation and interface trapped charge is eliminated. The desire for such monolithic structures is long-standing; a ferroelectric field effect transistor (FFET) has been envisioned[1-3] as a major technological innovation, but its development has been hindered by the lack of a fundamental understanding of how to control interface chemistry and electrostatics between these materials.

The basic problem to be overcome in the growth of epitaxial oxides on a semiconductor like silicon is that silicon easily forms SiO_2 when exposed to an oxygen containing environment. Moreover, silica is amorphous, and once formed, masks the crystalline template of the underlying silicon surface. This problem is certainly well established, and for silicon there have been numerous methods used in trying to solve it; some have been merely scoping experiments, "try this, maybe it will work", but others have been more systematic. The systematic attempts have, for the most part, been centered on thermodynamic stability studies or reaction/reduction approaches to dealing with silica or silicate formation.

"The submitted manuscript has been authored by a contractor of the U.S. Government under contract No. DE-AC05-96OR22464. Accordingly, the U.S. Government retains a nonexclusive, royalty-free license to publish or reproduce the published form of this contribution, or allow others to do so, for U.S. Government purposes."

DISTRIBUTION OF THIS DOCUMENT IS UNLIMITED
MASTER

DISCLAIMER

Portions of this document may be illegible in electronic image products. Images are produced from the best available original document.

DISCLAIMER

This report was prepared as an account of work sponsored by an agency of the United States Government. Neither the United States Government nor any agency thereof, nor any of their employees, makes any warranty, express or implied, or assumes any legal liability or responsibility for the accuracy, completeness, or usefulness of any information, apparatus, product, or process disclosed, or represents that its use would not infringe privately owned rights. Reference herein to any specific commercial product, process, or service by trade name, trademark, manufacturer, or otherwise does not necessarily constitute or imply its endorsement, recommendation, or favoring by the United States Government or any agency thereof. The views and opinions of authors expressed herein do not necessarily state or reflect those of the United States Government or any agency thereof.

Barium titanate and lead titanate have received the most attention (for reviews and recent compilations see ref 4 and 5). However, there is a very practical distinction that is apparent for these perovskites that arises in the common practice of their MOCVD growth[6]. The usual precursors of barium and strontium (beta-diketonates) decompose to stable carbonates which require temperatures in excess of 650°C for conversion to oxides. This invariably leads to uncontrolled oxidation of the silicon[7]. Lead titanate has been used with greater success because deposition temperatures may be lowered to 500°C[8], but lead titanate and silicon react to degrade the properties of the ferroelectric layer[9]. This type of problem is really generic to all of the attempts at reaction/reduction for growing the perovskites on silicon[10], and variants on it that do not address the atomistic details and the electrostatics of the interface between a semiconductor and an ionic oxide will continue to be less than adequate. We have approached a solution of this problem by going to the fundamentals of metal silicide formation and, through the silicide, transitioning to crystalline oxide structures.

In what follows, we will summarize how the epitaxial growth of $BaSi_2$ occurs on the (001) and (111) faces of silicon. Moreover, we will show that cubic symmetry precursors to the orthorhombic polymorph of $BaSi_2$ can be stabilized on Si(001). We will then go on to describe the growth and interfacial electrostatics as a dominant influence on heteroepitaxy in perovskite oxides. Finally we will illustrate a unique structure for a commensurate $CaSrTiO_3$/Si interface that promotes the growth of highly perfect thin-film ferroelectrics. MOS capacitor data taken from these structures provide the conclusive demonstration that the FFET can be made.

Silicide/Oxide Heteroepitaxy on Silicon

The synthesis and processing of epitaxial silicides has a long standing utility in semiconductor and transistor technology. Nearly perfect structural matches between silicon and several transition metal silicides have been reported, and, as a result, systematic studies of the physics of epitaxy at metal-semiconductor interfaces have been performed [11]. However, not withstanding the breadth of the work that has been reported, there has been little effort directed toward understanding how a silicide structure plays a role in the heteroepitaxial transition between silicon and an overgrowing epitaxial oxide. To date, the primary motivation for epitaxial silicide studies has been to characterize electrical contact behavior in device structure development [12-14].

Our approach has been a study of the barium-silicon reaction and factors that govern epitaxial structure development of barium silicide on silicon for subsequent oxide growth[15]. The barium reaction and structure are typical of the alkaline earth metals; strontium, calcium, and magnesium all order commensurately on Si(001) at submonolayer coverages. We will show that the dominant feature controlling epitaxial development on both (001) and (111) silicon is the alkaline earth ordering along the <110> directions on the two surfaces. These submonolayer structures ($BaSi_2$ will be discussed in detail) are the templates for the heteroepitaxial transition to alkaline earth-containing oxides on silicon.

The barium-silicon phase diagram[16] is relatively simple and shows that two line compounds, BaSi and $BaSi_2$, form with limited-to-no solubility of either barium or silicon. The disilicide coexists with silicon above 840°C. While it might be possible to obtain this reaction product as a single phase at temperatures below 840°C, we have carefully avoided any possibility of the monosilicide formation by studying the epitaxy of $BaSi_2$ on both (001) and (111) planes of silicon at temperatures above 840°C (all of the thin film growth and characterization in this study were performed in an ultrahigh vacuum molecular beam epitaxy system).

Evers et al. [17,18] have systematically studied the thermodynamics and structures of bulk $BaSi_2$ in its orthorhombic, cubic, and triclinic polymorphs. The ambient pressure polymorph is orthorhombic; Pnma, with the $BaSi_2$-type structure [19]. The most prominent features of this structure are the isolated Si-tetrahedra separated from each other by more than 1.5 Si-Si bond distances. The silicon tetrahedra are only slightly distorted from their ideal bond angles of 60° with Si-Si bond distances of 0.239 nm (Si-Si distances in silicon are 0.235 nm). The isolated tetrahedra are interconnected by barium atoms and form (010) planar channels in the structure. Figure 1 shows a ball model of the structure viewed normal to a (100) plane; the model is one unit cell deep: large balls are barium, small ones are silicon. Although the structure is complicated, a simple crystal anisotropy manifested by (010) planar channels is particularly useful an understanding the growth mechanism of the silicide on silicon.

The lattice parameters for the orthorhombic phase suggest that good structural matching should occur on Si(111). The *c* parameter of $BaSi_2$ is 1.158 nm (three times the [110] spacing for silicon is 1.152 nm); the *b* parameter of $BaSi_2$ is 0.680 nm (three times the [112] spacing for silicon is 0.669 nm). This is the epitaxy that develops: $BaSi_2$(100)|Si(111) with $BaSi_2$<001>|Si<110>; three variants are, of course, obtained. Figure 2 shows RHEED patterns from the <010> and <001> zone axes of the $BaSi_2$(100) surface. The film quality is excellent with the flat surface giving rise to streaked RHEED patterns. While it might be expected that, with the orthorhombic structure of $BaSi_2$, both the (010) and (100) planes would grow parallel to Si(111), we do not observe anything but (100) growth. This may well be a consequence of the anisotropy of the diffusion process that must occur during the reactive epitaxy process; the silicide was grown at high temperatures by simply exposing the silicon surface to barium. As shown in Fig. 1, a projection of the $BaSi_2$ structure onto the (100) reveals rows of barium atoms that are the bridging elements between the isolated silicon tetrahedra. Stacking of these rows in (100) planes forms (010) planar channels through which silicon or barium can diffuse to react at the surface.

The same phenomena occur on the (001) surface of silicon; barium atoms order along the <110> directions of silicon forming the rows in the silicide structure, and epitaxy develops with $BaSi_2$(100)//Si(001) and $BaSi_2$<001>//Si<110>. RHEED patterns at a <110> zone axis of the silicon surface show the two variants of this epitaxial structure. Figure 3 is a RHEED pattern taken at a <110> zone axis of Si(001); this pattern reveals the <010> and <001> spacings of $BaSi_2$. Again, as with the (111) surface, the <100> axis of $BaSi_2$ is normal to the growth plane.

The observations of epitaxy on both (111) and (001) silicon show the propensity for the

silicide growth to be dominated by the lattice matching that occurs when $BaSi_2$<001> aligns with Si<110>. In both cases the silicide formed with its (100) plane parallel to the growth surface; the open channels of silicon tetrahedra are oriented normal to this plane. A transmission electron microscopy (TEM) image (reproduced from ref 15) of the silicide/silicon(001) interface viewed along a Si<110> direction is shown in Fig. 4. The variant that is imaged is a <001> zone axis of the $BaSi_2$ growing with the *a* axis normal to the surface. An image simulation and a structure model are shown as the insets in Fig. 4. The channels in the silicide structure are clearly illustrated as the white chains in the $BaSi_2$.

The study of the thick-film epitaxy described above illustrates that barium atoms order along the <110> directions of the silicon surfaces. This ordering developed at even submonolayer coverages and suggested that the high-pressure cubic polymorph of $BaSi_2$ might be stabilized by epitaxy on the (001) face of silicon. Cubic $BaSi_2$ adopts the $SrSi_2$ structure with a lattice parameter that is 11% larger than the 0.543 nm *a* constant for silicon [20]. The cubic unit cell contains four molecules, and a projection of one molecular unit onto a (001) face illustrates a slight distortion from a face-centered net. At low-surface coverages, barium reacts and orders along Si<110> commensurate with the silicon surface.

Figure 5 shows intensity vs coverage data accumulated for the (0,0), (1/3,0), and (1/2,0) rods of RHEED from the (001) silicon surface at a [110] zone axis. These data were obtained by digitizing RHEED screen images collected with a video camera. The dashed lines labeled "A" and "B" mark maxima in the specularly reflected (0,0) rod that occur at coverages of 1/6 and 1/4 monolayers (ML), 1 ML = 6.78×10^{14} atoms/cm^2. These maxima in the specular beam occur as the surface flattens when the ordered surface structures are complete. The other two curves in the figure, the (1/3,0) and (1/2,0) rod intensities, provide data that describe surface structural evolution as opposed to the surface morphological information contained in the specular rod.

The (1/3,0) rod intensity goes through a maximum at 1/6 ML, and the diffraction pattern, photo A in Fig. 5, shows the lattice parameter tripling. This intermediate state decomposes as barium deposition continues, but at 1/4 ML, the (1/2,0) rod goes through a strong maximum, and the diffraction pattern, photo B in Fig. 5, shows a highly ordered surface. We believe that the (1/2,0) rod is evidence of a strain-induced stabilization of cubic $BaSi_2$: a 45° rotation of the $BaSi_2$ on (001) silicon would place a barium atom in every other silicon site along the <110> of the surface. Moreover, a 1 ML surface of cubic $BaSi_2$ is equivalent to the 1/4 ML coverage based on the silicon surface. If barium deposition is continued, the 2 x 2 surface collapses to the orthorhombic bulk $BaSi_2$ for coverages greater than one ML. XPS analyses of both the 3 x 3 and 2 x 2 surfaces show that the Ba-3d photoelectron peak and the x-ray excited Auger transitions are shifted to barium silicide states relative to a barium metal standard. The 2 x 2 surface obtained at 1/4 ML coverage provides a template that can be used to grow BaO epitaxially on silicon. Strontium illustrates these same ordered structures at the same coverages as barium. These high-temperature ordered submonolayer structures are stable on cooling to room temperature. Subsequent barium or other alkaline earth metal deposition onto this surface at low temperatures does not react to form a silicide. The transition to a heteroepitaxial, alkaline earth-containing oxide can be accomplished directly from this silicide template structure [21].

Electrostatics and the Stability of A Single Orientation Alkaline Earth Oxide/Perovskite interface

We have discussed how the interface between silicon and the alkaline earth oxide is developed, but the transition to the perovskite from the alkaline earth oxide must be understood in order to grow the ferroelectric phase. While it is not possible in the present context to describe in detail the characterization of the interface structure, the basic features are summarized as follows: For a heteroepitaxial transition between insulating oxides, the interface electrostatics (ion-ion near-neighbor interactions) of the first layers critically determine whether a commensurate structure can develop. We have discussed this at some length[22]. That discussion and its relevance in the present problem is summarized in the following using the $MgO/BaTiO_3$ interface as an example; it is typical of the oxides in this system.

To appreciate how the interfacial electrostatics issue arises, we only need to consider the structure of the perovskite oxides. The distinguishing structural characteristic of the perovskite oxide class is recognized as a closest-packing of large cations and oxygen anions arranged as stacked sheets normal to a [111] direction. The octahedral interstices that form as a result of this sheet-stacking sequence are in turn filled with higher valence, smaller cations. The resulting structures are cubic with low-index stable crystal faces. The naturally occurring crystal truncations are {001} and are then, for example with $BaTiO_3$, either BaO planes or TiO_2 planes. The ion sizes and charges in these planes are distinctly different, and the initiation of a heteroepitaxial growth sequence for such a structure on another insulating oxide must take this into account.

Figure 6 provides an illustration of the favorable result that can be obtained if the growth sequence for the transition to the perovskite is initiated in the $BaTiO_3$ unit cell at the TiO_2 plane. A commensurate, atomically flat layer of TiO_2 can form in which every other cation row is vacant over the underlying Mg^{2+} sites. This TiO_2 truncation of (001) MgO satisfies the electrostatic requirements for anion-cation near-neighbor pairs at the interface and is a low-energy, stable truncation of the MgO surface. The missing row of cations in this layer provides the energetically favorable sites for subsequent barium-ion attachment to the crystal surface. The transition from heteroepitaxy to homoepitaxy of the perovskite is completed with the desired single-orientation material and its advantageous long-range structural coherence.

$CaSrTiO_3$/Si and $BaTiO_3$

Within our discussion in the preceding sections, we have outlined how commensurate silicide formation is accomplished on (001)Si, and we have reviewed the idea that electrostatics at ionic oxide interfaces can be controlled. Our goal is to truncate silicon with a stable perovskite structure that will allow us to grow a thin-film ferroelectric on silicon as a monolithic structure. Figure 7 is a RHEED pattern taken from the surface of $Ca_{0.66}Sr_{0.34}TiO_3$ grown on (001)Si. The film is only 3.5 unit cells thick; is lattice matched and commensurate to the 5.43Å silicon surface; but is rotated 45° so that the

[001] of the film is parallel to the [110] of silicon.

This structure is grown using source shuttering from effusion cells in a conventional MBE system, and the composition is chosen as a simple linear mixing of the Ca and Sr in the AO layer of the ABO_3 perovskite structure. It is a member of our general series of commensurate structures designated as $(AO)_n(A'BO_3)_m$ in which n and m are the integer repeats of single-plane commensurate oxide layers. If n = 1 then the perovskite is grown directly as ABO_3 from the silicide truncation of silicon beginning at the AO plane. If n > 1, the face-centered NaCl-type structure is grown at the interface, then truncated with the BO_2-plane to transition to the perovskite structure. Figure 8 is a cross section of a scanning tunnelling electron microscopy image (STEM) of the near interface region of our $(AO)_n(A'BO_3)_m$ structure series. This example uses $n = 5$ and $m = 4$; the AO_n layers are $Ba_{0.73}Sr_{0.27}O$ having a lattice parameter of 5.43Å; and the $A'BO_3$ layers are $Ca_{0.66}Sr_{0.34}TiO_3$ having a 3.84Å lattice parameter to match the (110) spacing for a 45° rotation.

The STEM image is distinct from a conventional phase contrast TEM image. It is a Z-contrast image that is atomic number (Z) sensitive and directly represents the chemical and structural characteristics of the interface. The first bright layer at the interface is the silicide layer containing the heavier barium atoms, the transition in the next 4 layers is the $Ba_{0.73}Sr_{0.27}O$ fcc structure with a cube-on-cube relationship to silicon, and finally the 45° perovskite rotation of $Ca_{0.66}Sr_{0.34}TiO_3$ is shown. This structure is monolithic, lattice matched and commensurate to the underlying (001) silicon surface; it completely avoids amorphous silica formation. With this commensurate interface on silicon the ferroelectric perovskites can be subsequently grown to any desired thickness.

Figure 9 contains capacitance/voltage and leakage current data taken using a simple capacitor circuit composed of our $(AO)_n(A'BO_3)_m$ structure with n and $m = 4$, an overgrown 280Å thin-film of $BaTiO_3$, and silicon. The characteristic dip in the capacitance data occurs as the silicon goes from accumulation to depletion[23]. The resistivity taken from the ohmic region of the leakage current curve is 10^{13} ohm-cm, and the leakage current is less than 10^{-9} amps/cm^2 at 2 volts. These results are unparalleled for thin-film perovskite capacitors on silicon[2-5].

Conclusion

We have shown that submonolayer silicides are the template surface structures that promote the heteroepitaxial growth of perovskite ferroelectrics on silicon. A unique structural series of alkaline-earth oxide/perovskite oxide layers has been identified that forms a monolithic $Si/(AO)_n(A'BO_3)_m$ interface. This interface is devoid of any amorphous Si-containing oxide and allows, for the first time, a true synergism of ferroelectric and semiconductor properties. This synergism illustrates that the demanding high resistivity, low-leakage current capacitors that are the required elements of a ferro-gated technology can be grown in a controlled and reproducible manner.

Acknowlegments:

Research sponsored jointly by the Laboratory Directed Research and Development Program of Oak Ridge National Laboratory, and by the Division of Materials Sciences, U.S. Department of Energy under contract DE-AC05-96OR22464 with Lockheed Martin Energy Research Corporation.

References

1) D.H. Looney, U.S. Patent No. 2791758(1957); W.L. Brown, U.S. Patent No. 2791759(1957); I.M. Ross, U.S. Patent No. 2791760(1957); J.A. Morton, U.S. Patent No. 2791761(1957).
2) Y. Watanabe, *Appl. Phys. Lett.* **66**, 1770(1995).
3) M.W.J. Prins, K.O. Grosse-Holz, G. Muller, J.F.M. Cillessen, J.B. Giesbers, R.P. Weening and R.M. Wolf, *Appl. Phys. Lett.* **68**, 3650(1996).
4) "Special issue, Ferroelectrics", *JJAP* **35**, No 9B(1994).
5) "Special issue, Electroceramic Thin Films", *MRS Bull* **21**, No. 7(1996).
6) D.B. Beach, private communication (1996).
7) S.R. Gilbert, B.W. Wessels, D.A. Neumayer, T.J. Marks, J.L. Schindler and C.R. Kannewurf, *Mat. Res. Soc. Symp. Proc.* **335**, 41(1994).
8) H.Chen, B.M. Yen, G.R. Bai, D. Liu and H.L.M. Chang, *Mat. Res. Soc. Symp. Proc.* **335**, 35(1994).
9) Y. Shichi, S. Tanimoto, T. Goto, K Kurowa and Y. Tarui, *JJAP* **33** part 1, 5172(1994).
10) Y. Kado and Y. Arita, J. Appl. Phys. **61** 2398(1987); H. Mori and H. Ishiwara, *JJAP* **30**, L1415(1991).
11) R. T. Tung, J. M. Poate, J. C. Bean, J. M. Gibson, and D. C. Jacobson, *Thin Solid Films* **93**, 77, (1982).
12) J. M. Phillips, in *Silicon-Molecular Beam Epitaxy*, edited by E. Kasper and J.C. Bean (CRC, Boca Raton, FL, 1988), Vol. 1, p. 135.
13) J.C. Bean, in *Silicon-Molecular Beam Epitaxy*, edited by E. Kasper and J.C. Bean (CRC, Boca Raton, FL, 1988), Vol. 2, p. 65.
14) M. Akiyama, K. Kawarada, S. Hishi and K. Kaminishi, Materials Research Society Meeting, Palo Alto, Calif., April 1986.
15) R.A. McKee, F.J. Walker, J.R. Conner and R. Raj, *Appl. Phys. Lett.* **63**, 2818(1993).
16) T. B. Massalski, J. L. Murray, L. H. Bennett, and H. Baker, *Binary Alloy Phase Diagrams* (American Society for Metals, Metals Park, Ohio, 1986), Vol. 1.
17) J. Evers, J. Less-Common Met. **58**, 58 (1978).
18) J. Evers, J. Less-Common Met. **69**, 399 (1980).
19) K. H. Janzon, H. Schafer, and A. Weiss, Z. Anorg. Allg. Chem. **372**, 87 (1970).
20) A. F. Wells, *Structural Inorganic Chemistry* (Clarendon Press, Oxford, UK 1975), p. 498.
21) R. A. McKee, F. J. Walker, J. R. Conner, and E.D. Specht, Appl. Phys. Lett. **59** (7), 782(1991).
22) R.A. McKee, F.J. Walker, E.D. Specht, G.E. Jellison, Jr., L.A. Boatner and J.H. Harding, *Phys. Rev. Lett.* **72**, 2741(1994).
23) Narain Arora, *MOSFET Models for VLSI Circuit Simulation - Theory and Practice* (Springer-Verlag, New York, 1993), Chapter 4.

Figure Captions

Figure 1. A one-unit-cell projection of $BaSi_2$(100); the channels in the structure are viewed edge on and are in (010) planes. Large balls are barium, small ones are silicon.

Figure 2 RHEED patterns from BaSi2(100); film thicknesss, 20 nm

Figure 3 RHEED pattern for BaSi2(001); film thickness, 20 nm

Figure 4 TEM image of silicide/silicon interface, Si<110> -Si(001). Viewing direction is Si<110>//$BaSi_2$<001>. The simulated image is obtained with a defocus of -45 nm and thickness of 5 nm.

Figure 5 Ordered surface RHEED patterns for submonolayer coverages. Rod notation is based on surface unit mesh; zone aixs is three-dimensional convention.

Figure 6 TiO_2 truncation of (001)MgO. (a) RHEED at the [100] zone axis for clean and TiO_2-truncated MgO; (b) ball models of (001) surfaces.

Figure 7 RHEED pattern at [100] zone axis of (001) surface of $Ca_{0.66}Sr_{0.34}TiO_3$ lattice matched and commensurate to (001) Si. The film is 3.5 unit cells thick.

Figure 8 STEM image looking down the [110] zone axis of silicon. The $Ba_{0.73}Sr_{0.27}O$ is cube- on-cube; the $Ca_{0.66}Sr_{0.34}TiO_3$ rotated 45°. The structure insert is based on n=5 and m = 4 in the structure series notation $(AO)_n(A'BO_3)_m$. The crystalline silicon substrate and commensurate $(AO)_n(A'BO_3)_m$ thin-film are capped with amorphous silicon for the STEM sample.

Figure 9 $BaTiO_3$ MOS capacitor on p-doped silicon. The upper panel is Quasistatic Capacitance vs gate voltage; the lower panel is leakage current vs gate voltage. The data are taken 160 um dia. aluminum pads with aluminum electrodes on the back side of the silicon.

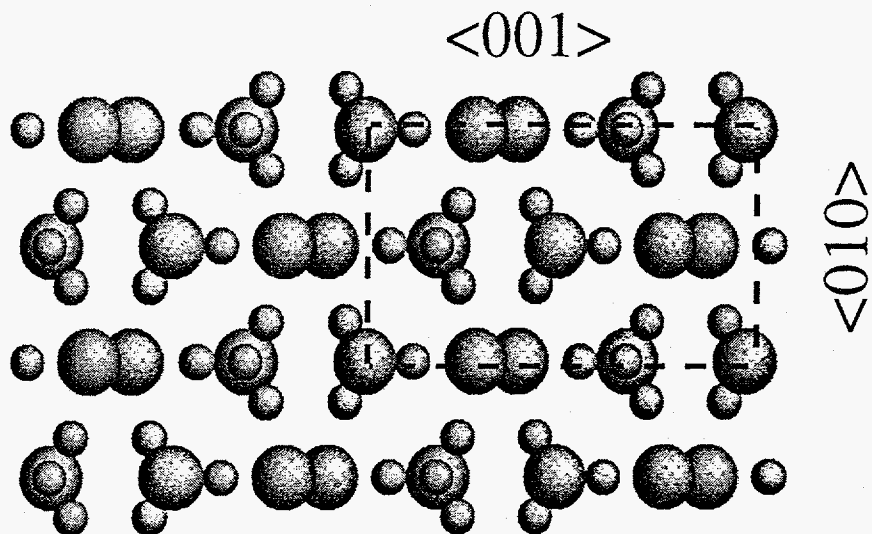

Figure 1. A one-unit-cell projection of $BaSi_2$(100); the channels in the structure are viewed edge on and are in (010) planes. Large balls are barium, small ones are silicon.

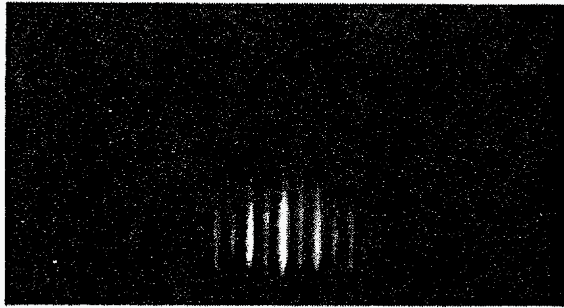

$BaSi_2$ <010>

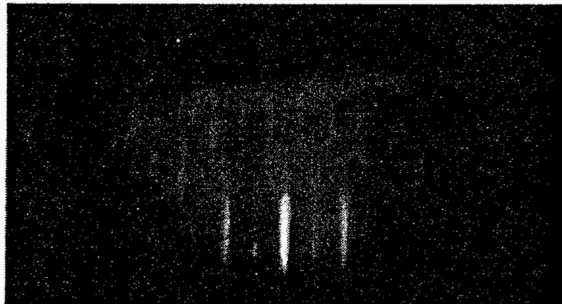

$BaSi_2$ <001>

Figure 2 RHEED patterns from BaSi2(100); film thicknesss, 20 nm

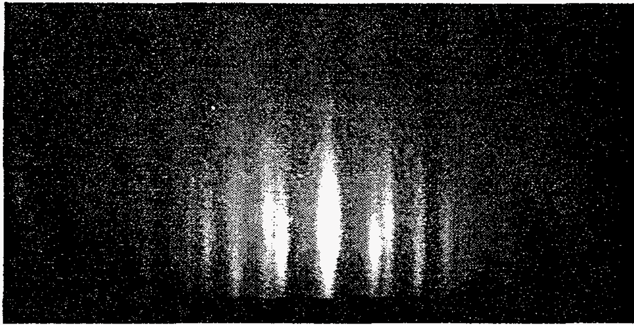

$BaSi_2$ <010> *and* <001>

Figure 3 RHEED pattern for BaSi2(001); film thickness, 20 nm

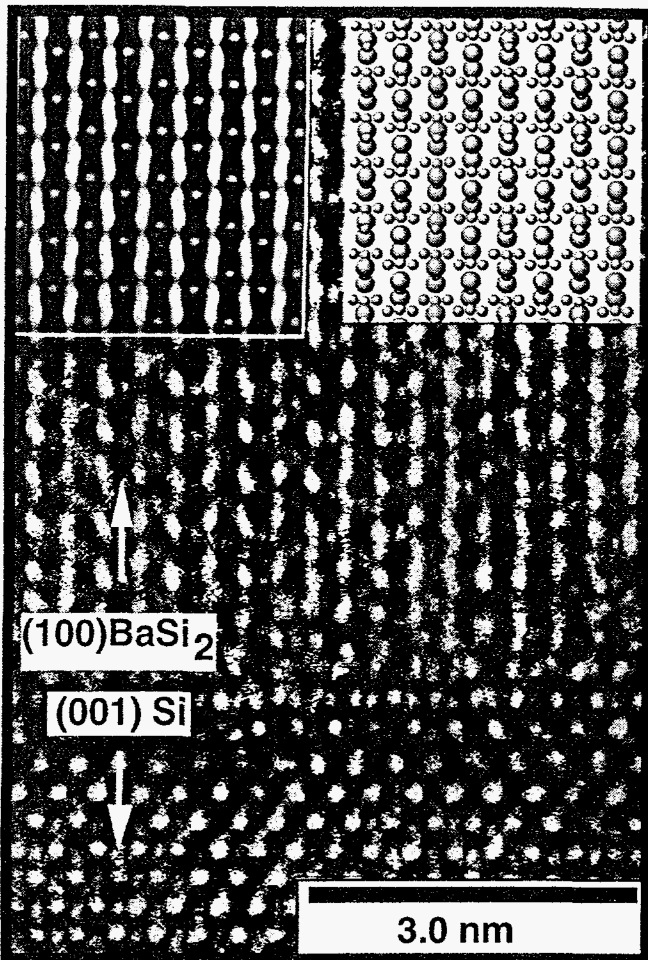

Figure 4 TEM image of silicide/silicon interface, *Si<110>* -Si(001). Viewing direction is Si<110>//$BaSi_2$<001>. The simulated image is obtained with a defocus of -45 nm and thickness of 5 nm.

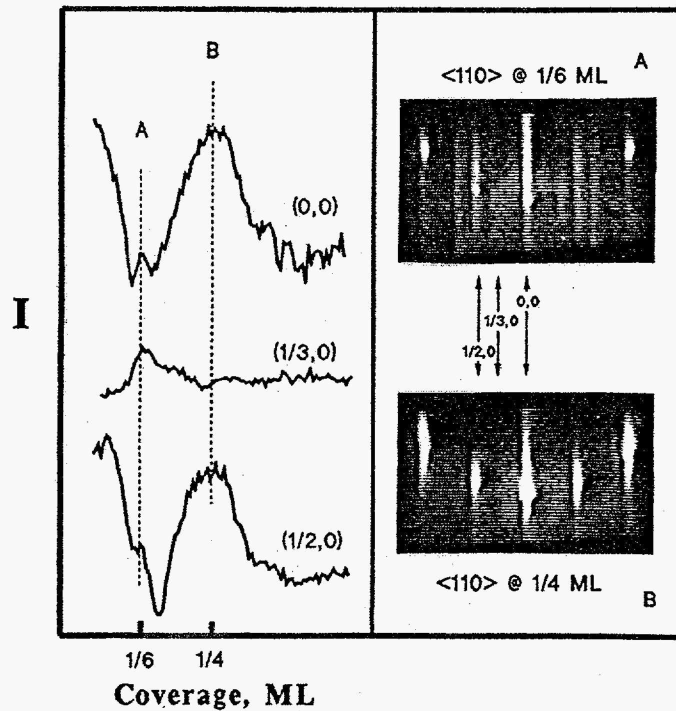

Figure 5 Ordered surface RHEED patterns for submonolayer coverages. Rod notation is based on surface unit mesh; zone aixs is three-dimensional convention.

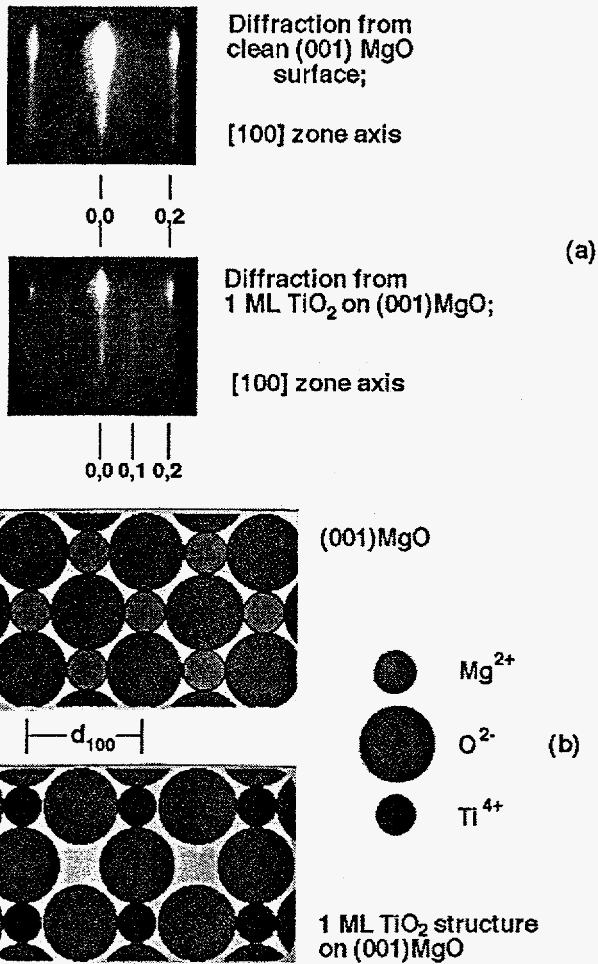

Figure 6 TiO2 truncation of (001)MgO. (a) RHEED at the [100] zone axis for clean and TiO2-truncated MgO; (b) ball models of (001) surfaces.

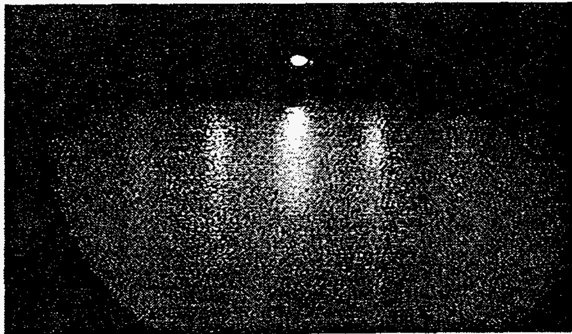

Figure 7 RHEED pattern at [100] zone axis of (001) surface of $Ca_{0.66}Sr_{0.34}TiO_3$ lattice matched and commensurate to (001) Si. The film is 3.5 unit cells thick.

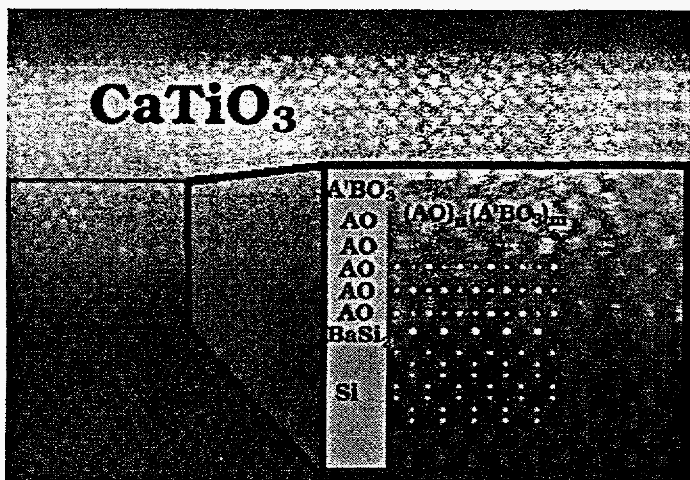

Figure 8 STEM image looking down the [110] zone axis of silicon. The $Ba_{0.73}Sr_{0.27}O$ is cube- on-cube; the $Ca_{0.66}Sr_{0.34}TiO_3$ rotated 45°. The structure insert is based on n=5 and m=4 in the structure series notation $(AO)_n(A'BO_3)_m$.

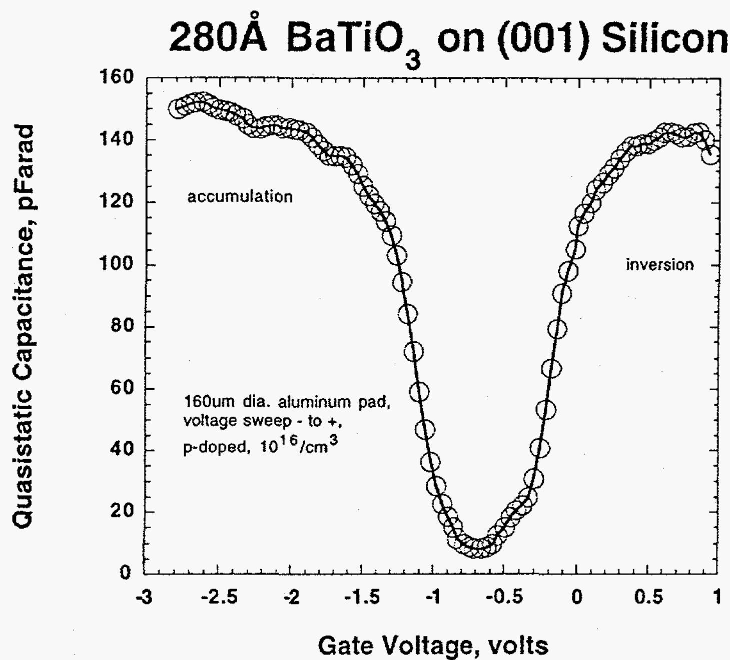

(a)

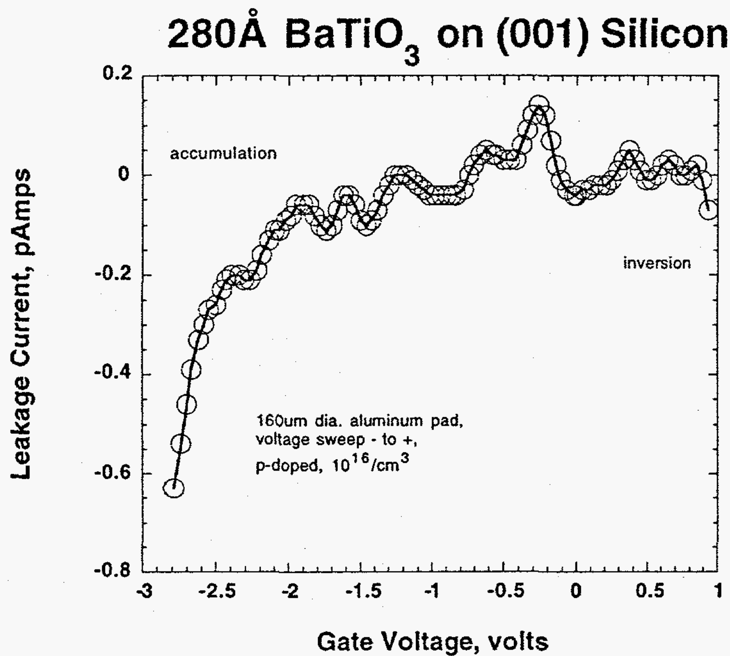

(b)

Figure 9 $BaTiO_3$ MOS capacitor on p-doped silicon. The upper panel is Quasistatic Capacitance vs gate voltage; the lower panel is leakage current vs gate voltage. The data are taken 160 um dia. aluminum pads with aluminum electrodes on the back side of the silicon.